5-2019

Spatial Encoding with Single-sided NMR

Madeline Brass

Spatial Encoding with Single-sided NMR

Madeline Brass

April 22, 2019

Spatial Encoding with Single-sided NMR

A thesis submitted in partial fulfillment of the requirement
for the degree of Bachelor of Science in Chemistry from
The College of William and Mary

by

Madeline Brass

Accepted for HONORS
(Honors, High Honors, Highest Honors)

Tyler Meldrum, Director

John Pontsma

Christopher Abelt

Jonathan Frey

Williamsburg, VA
April 22, 2019

Abstract

Single-sided NMR is an important non-invasive, non-destructive technique used to characterize molecules. Specifically, single-sided NMR has applications in biomedicine, elastomers, solid polymers, moisture in porous media, and cultural heritage. Single-sided magnets can be used to analyze T_2 relaxation to gauge the relative motion of molecules in the sample. However, the are few methods to characterize heterogeneous samples with single-sided NMR. Most experiments take one set of data for the entire sample regardless if the sample is heterogeneous or homogeneous. New methods to spatially encode with single-sided NMR were explore and characterized based on their advantages and disadvantages. These methods include hard pulses, profiles, soft pulses, and Hadamard sequencing. The methods discretely selective excite specific regions of the sample. The T_2 relaxation is measure for each slice within the sample allowing for characterixation of heterogenous samples.

Acknowledgements

I would like to thank Tyler Meldrum for his continuous support throughout my undergraduate research and specifically the work on this project. I am grateful for all he has taught as a student and researcher as this would not have been possible without him. I would also like to thank the Meldrum Lab Group for creating an enjoyable environment to work in, specifically Mackenzie Kelly (current graduate student) and Mary Rooney (former graduate student) for taking time to edit my thesis. I would like to thank the Chemistry Department and The College of William & Mary for giving me this opportunity. Finally, I am especially grateful to my study group, Anwar Radwan, Davis Gold, Miguel Locsin, and Alfredo Fallorina for their assistance with chemistry studies outside the lab and encouragement for my research.

Broader Impacts

Traditional NMR is a very popular and useful technique used to determine molecular structure. However, it provides disadvantages in that it is a destructive and invasive technique. Traditional NMR cannot be used in cases where the sample needs to be preserved. Single-sided NMR is advantageous in that it is a non-destructive and non-invasive technique. However, there is some hesitancy to use this technique, because it is not as sensitive and powerful as traditional NMR. This study aims refine single-sided NMR techniques to broaden and amplify its applications. This is accomplished by characterizing the sample in discrete positions as small as in 50 µm, which has a wide range of applications.

Applications of single-sided NMR fall within biomedicine, elastomers, polymers, porous media, and cultural heritage. Within cultural heritage, single-sided NMR can be used to characterize the paints in artwork. The advantage is that the magnet can be brought to the painting for characterizations, so they painting does not need to be moved or touched. These specific methods can be used to analyze the different paint layers individually. Another application withing biomedicine is the use of single-sided NMR to gauge degradation in the Achilles tendon. The Achilles tendon is a dense collegen structure that cannot be analyzed with tradition NMR. However, a single-sided magnet can be oriented properly with relation to the Achilles tendon that allows for characterization. Finally, a third application of these methods is to characterize different layers of the skin. There is difficulty characterizing these layers separately, because they are so thin. However, this study improved techniques to get high sensitivity with smaller layers allowing for improved characterization of the skin layers. These are just a few applications of single-sided NMR and spatial encoding. The techniques will not only benefit studies in the specific lab, but within the entire single-sided NMR community.

Contents

List of Figures

1 Introduction

1.1 Background of Single-sided NMR

Nuclear Magnetic Resonance (NMR) is a powerful tool for determining molecular structure with applications in chemistry, physics, biology, and medicine. Some specific applications include biomedicine, elastomers, solid polymers, porous media, and cultural heritage. Specifically, single-sided NMR can be used to investigate the Achilles tendon *in vivo* and provides advantages traditional NMR does not provide. Because the achilles tendon has a dense collagen structure, when placed parallel to the magnetic field, little or no signal is observed. However, when the tendon is between 40° and 70° to the magnetic field, the NMR signal can be measured. Tradition clinical NMR imagers can not accommodate orientation specific imaging, but the single-sided NMR does, which can asses the condition of the tendon and any degenerative changes [1].

Single-sided NMR can also be used to differentiate between different layers of the skin, which can be helpful in identifying the best time and locations for taking biopsy samples as well as detect fluid content changes in different dermal layers [2].Alternatively, the degree of cross linking density in polymers can be measured with single-sided NMR non-invasively and non-destructively. This is useful to determine the quality of polymers and the functionality of the adhesives and resin-based components [3]. Finally, single-sided NMR is crucial to cultural heritage research, because the sample does not need to be moved or touched. For example, single-sided NMR can be used to identify thickness and type of paint layers in a painting as well as identify the binders used in the paint and primer, which are integral in studying what causes paint degradation as well as how to best preserve the painting [4] [5].

1.2 Instrumentation

In this study, two single-sided mangets are used, the PM25 and the PM5 by Magitrek. They are both small, single-sided, low field NMR-MOUSE magnets. These magnets are comprised

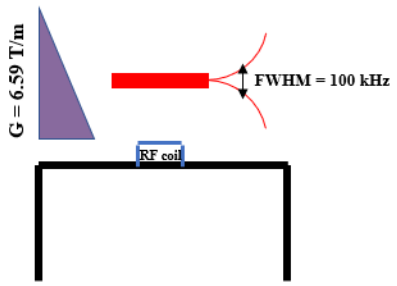

(a) Alignment of RF coil and magnetic field

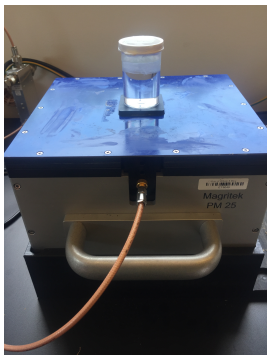

(b) PM25 magnet with glycerol sample

Figure 1: Figure (a) represents the orientation of the magnet, gradient, and magnetic field. The RF coil sits in the middle of the magnet and the purple triangle is the gradient (6.59 T/m) above the magnet.The RF coil is tuned to 13 MHz (where the red box is centered) and the farther from the center, the less sensitive the RF coil is in this region represented by the red lines. This sensitive region has a full width half max (FWHM) of 100kHz, corresponding to the sensitive region, which is depicted by the red box. Figure (b) is a picture of the PM25 with a glycerol sample on top.

of two magnet heads with a radiofrequency (RF) coil that defines the maximum penetration into the sample. The PM5 is accompanied by a Kea spectrometer created by Magitrek and the PM25 is accompanied by a SCOUT spectrometer created by *Tecmag*. Figure 1 displays the orientation of the PM25 magnet, RF coil, gradient, and magnetic field. The magnet has a gradient of 6.59 T/m and operates at 13 MHz. The farther away from the center of 13 MHz, the sensitivity of the RF coil decreases (as shown by the red lines). This sensitive region has a full width half max (FWHM) of 100 kHz. Both magnets are accompanied by an RF power amplifier. On the PM5, the software, *Propspa*, is used to generate pulses and receive data and the magnet operates at a frequency of 20 MHz. Alternatively, on the PM25, the software, *TNMR*, is used to generate and and receive pulse sequences and operates at a frequency of 13 MHz. In *TNMR*, the amplitude of the pulse and phase can be manually inserted to fit the experiment.

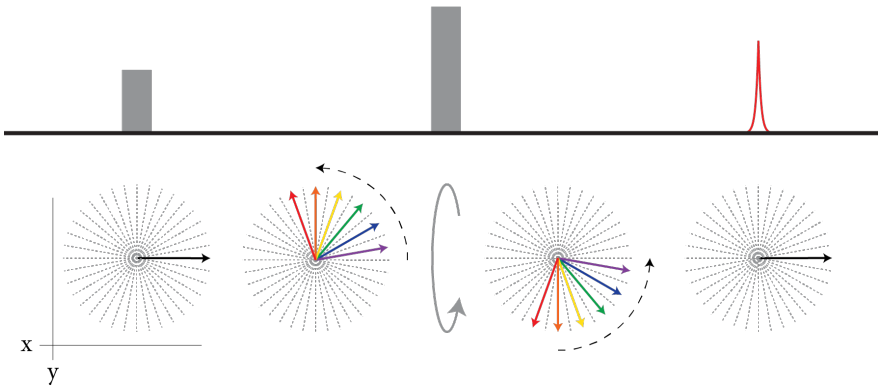

Figure 2: Pulse sequence used to generate an echo. Following the first 90° pulse, the spins are aligned with the transverse plane. There is some time of free induction decay before the 180° pulse which rotates the spins in the opposite direction on the transverse plane. The spins re-phase and an echo is detected. Photo credit Tyler Meldrum.

1.3 T_2 Relaxation

Although traditional NMR is considered one of the most powerful tools to elucidate molecular structure, it is an invasive technique and magnets cannot be brought to the sample site. Single-sided NMR is advantageous because it is a non-destructive technique and can be transported relatively easily to the sample site. Single-sided magnets can be used to characterize relaxation within a molecule, specifically T_2 relaxation, also known as spin-spin (transverse), which quantifies the amount of time it takes transverse magnetization to decay in the $x - y$ plane.

Each electron spin, a quantum mechanical form of angular momentum, has a magnetic moment, which has a magnitude that can point in any direction and an angle between the moment and the applied magnetic field (B_0). When a magnetic field is applied to molecules, a net magnetization occurs because slightly more spins will align with the magnetic field (parallel) than opposing the magnetic field (anti-parallel). The spins will precess around the magnetic field based on the angle of their magnetic moment. The precessing spins rotate around the applied magnetic field in a cone shape at the Larmor frequency, which depends on the type of nucleus and the strength of (B_0). In addition to the magnetic field, there are local fields created by each spin individually. Each spin generates its own magnetic field;

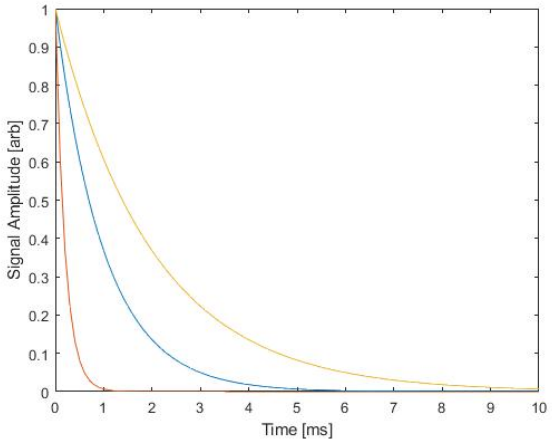

Figure 3: Each line represents a different T_2 relaxation rate fitted to the equation, $f(x) = e^{-ax}$ where $T_2 = 1/a$. The red line has a T_2 of 0.5 ms. The blue line has a T_2 of 1 ms.The yellow line has a T_2 of 2 ms.

.

therefore, every spin is experiencing the magnetic field of the spins around them. The local field is much weaker than the applied field and varies in amplitude and orientation as the molecules move [6].

Figure 2 represents the process by which T_2 is measured. When a radiofrequency (RF) pulse is applied to the sample, the spins will rotate towards the transverse plane $(x - y)$ plane. After a 90° pulse, the magnetic moment is aligned with the $x - y$ plane and the spins are precessing about the $x - y$ plane at the Larmor frequency. This first pulse generates free induction decay (FID). This is followed by a series of 180° pulses, which refocuses the spins. Both magnetic field inhomogeneity and chemical shift anisotropy contribute to transverse relaxation. The applied magnetic field is sometimes slightly shifted, which causes the magnetic field inhomogeneties and relaxation. Chemical shift anisotropy refers to the combination of the applied field and local field, which depends on the orientation of the molecule. The local field varies in direction and size for each molecule. Both of these factors contribute to the decay of magnetization in the transverse plane and are characterized by T_2

Following each 180° pulse is an echo where signal is detected. The signal intensity of the echo will decay over time. This decay can be fit to the exponential function $f(x) =$

e^{-ax} where $T_2 = 1/a$. Molecules with a small T_2 will decay faster and have a steeper exponential function. Figure 3 displays the decay of three different T_2 relaxations. The blue line represents molecules with a T_2 of 1 ms The red line with a steeper slope has a T_2 of 0.5 ms and the yellow line has a T_2 of 2 ms. [7]

T_2 is important to characterize because it gauges relative motion among molecules. Small, rapidly moving molecules, such as water, have larger T_2 values whereas larger, slower moving molecules, such as proteins, have smaller T_2 values. An example of an application for T_2 relaxation is that it can be used to gauge cross linking as a polymer cures. As polymers cure, there is more cross linking and less relative motion between the molecules, corresponding to a smaller T_2. The T_2 measurements can provide information about the rigidity of the molecular network[8].

1.4 Background of Spatial Encoding

The goal of this study is to analyze different methods to spatially encode with single-sided NMR. Traditional single-sided NMR experiments collect one set of data for the entire sample. Collecting one set of data for the entire sample assumes the sample is homogeneous or ignores that the sample is not homogeneous. However, spatially encoded single-sided NMR provides lateral spatial resolution for heterogeneous materials. In this study, different methods are used to discretely characterize different slices in the sample, including altering the size of the slice as well as moving the slice. The T_2 relaxation can be measured for each slice uniquely.

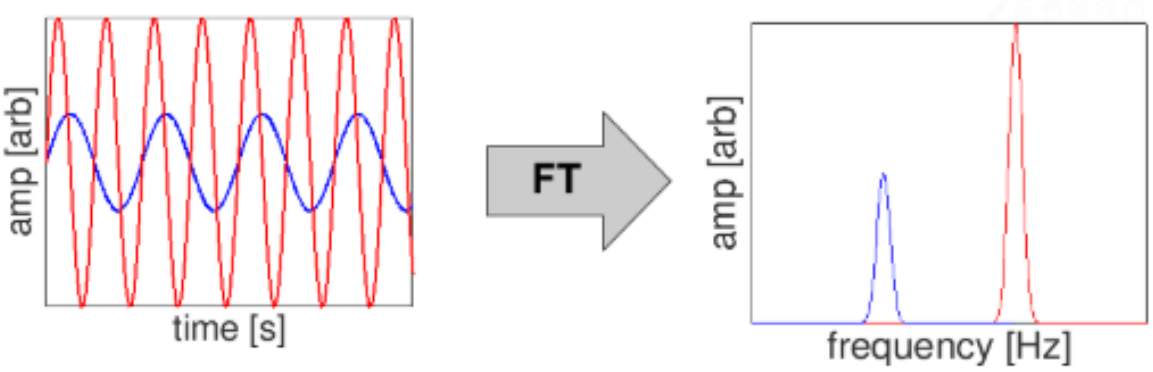

Figure 4: Two sine waves with different amplitudes and periods in the time dimension Fourier transform into two peaks in the frequency dimension. The red sine wave has a larger frequency and amplitude compared to the blue sine wave.

2 Theory

2.1 Fourier Transform

The Fourier transform is a mathematical operation used to analyze spectral data and represent different continuous parts of the signal. The continuous one-dimensional Fourier transform of a function $f(x)$ can be described as:

$$X(f) = \int_{-\infty}^{\infty} x(t) e^{-i2\pi ft} dt \tag{1}$$

The function $X(f)$ is the frequency spectrum of $x(t)$ where f is frequency and t is the time[9]. The function $f(x)$ is broken into its sinusoidal and cosinusoidal components at each unique frequency. If $x(t)$ contains only oscillations at one particular frequency, $X(f)$ will contain a single peak at that particular frequency. However, if the signal in $x(t)$ contains a superposition of multiple frequencies, $X(f)$ will display peaks at each of those frequencies. Not only does the discrete Fourier transform reveal periodicities in the data, but also amplitudes of these specific components. Figure 4 displays the Fourier transform of two basic sine functions. In the time domain, the function represented by the red line has a shorter period and larger amplitude. After the Fourier transform, the function represented

by the red line has a higher frequency and larger amplitude. In contrast, in the time domain, the function represented by the blue line has a longer period and smaller amplitude. After the Fourier transform, the sine wave represented by the blue line has a smaller frequency and amplitude. There are other important Fourier transform pairs to note, including the rectangular and SINC functions. The rectangular function is defined as $rect(x) = \Pi(x)$ where:

$$\Pi(x) = \begin{cases} 0 & if|x| > 1/2 \\ 1 & if|x| \leq 1/2 \end{cases}$$

and the SINC function is defined as: $sinc(x) = \frac{sin(x)}{x}$ (where $sinc(0) = 1$). The Fourier transform of the rectangular function is a SINC function. Inversely, the Fourier transform of a SINC function is a rectangular function [10].

2.2 Characteristics of a Pulse

There are a few important characteristics of a pulse. Every pulse is associated with some pulse length (typically in µs) that defines how long the RF power is transmitted through the RF coil. Alternatively, there is a bandwidth (typically in µm) that defines how big the region of excitation is. The pulse length and bandwidth of excitation are inversely proportional via the equation:

$$\Delta f = 1/t \tag{2}$$

where

$$f(Hz) = B_0 * \gamma * \text{bandwidth(mm)} \tag{3}$$

The variable t is the pulse length and f is the bandwidth converted from µs to Hz [11]. When exciting smaller regions, longer pulse lengths are used. Inversely, when exciting larger regions, smaller pulse lengths are used. Long and short pulses provide unique advantages

and disadvantages.

Another property of the RF pulse is its phase. The phase of the RF pulse is the angle between the desired polarization and the applied magnet field. For a 90° pulse, the phase is 90° when the pulse is being emitted. After the pulse is applied, there is a signal collection period, where an echo is detected. A combination of a 180° pulse and an echo is a spin-echo.

The magnetic field (B_1) applied by the RF coil rotates around the static field at some carrier frequency. This carrier frequency is tuned to characterize the center frequency of the magnetic field. Pulses are emitted and received at the carrier frequency. The sensitivity of the excitation and receiving bandwidth is also limited by the RF coil, which can excite and receive a 350 µm range. This range is centered at the carrier frequency. On some magnets, the coil can be tuned to alter the excitation bandwidth and center, however, the magnets used in this study cannot be tuned.

2.3 Hard Pulse

A hard pulse is a short, high power pulse that typically excites a large region of the sample. These pulses are in the shape of a rectangular function in the time domain. The pulse length (τ),which determines the size of the excitation region, is typically on the order of µs. For a 90° excitation pulse on the magnets used for this experiment, the pulse length is 6 µs with an amplitude of 26. The amplitude represents the amount of power emitted by the RF coil. These parameters are calibrated for the magnet and flip the magnetization vector 90° from the applied magnetic field. Alternatively, for a 180° pulse, the amplitude is 52 with a pulse length of 6 µs. These excitation pulses are common in spin-echo pulse sequences, particularly the *Carr-Purcell-Meiboom-Gill* (CPMG) pulse sequence [12].

As shown in Figure 5, this pulse sequence is comprised of a 90° excitation pulse, with a 180° pulse and free induction decay (FID) repeated. The initial 90° pulse flips the spins to precess around the $x - y$ plane. The 180° flip refocuses this pulse to form a series of detectable echoes. The CPMG pulse sequence is used to measure T_2 relaxation. In these

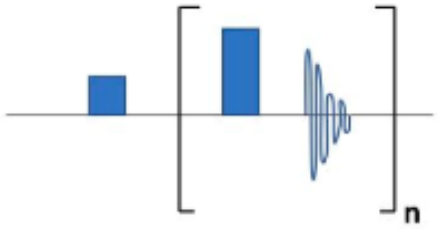

Figure 5: A CPMG pulse sequence comprised of a 90° flip and iterations of 180° flips with free induction decay.

experiments, a 30 µm region is excited and detected with a CPMG pulse and is used as a frame of reference for other pulse sequences. When exciting large regions, such as 350 µm, the CPMG pulse sequence is sufficient. However, when exciting smaller regions, such as 50 µm, hard pulses are not sufficient. A hard pulse in the shape of a rectangular functions yields a SINC function after Fourier transform. The SINC shpae is depicted in 6 A shorter rectangular pulse corresponds to a broader SINC function, whereas longer hard pulses excite a narrower region. For smaller excitation regions, there is not uniform excitation due to the shape of the SINC pulse. Hard pulses are not sufficient for selectively exciting smaller regions in the range of 50 µm to 200 µm. Instead, soft pulses are used to selectively excite smaller regions.

2.4 Soft Pulses

Soft pulses are long, shaped pulses and are better suited for slice selection [13]. For the experiments in this study, these pulses are typically 50 µs to 500 µs long and excite a region from 50 µm to 200 µm. The SINC pulse is comprised of lobes, with a center lobe of maximum amplitude surrounded by smaller lobes. Each lobe is half the width of its neighboring lobe to the center. The Fourier transform of an infinitely long SINC pulse is a rectangular function. However, experiments are run with truncated SINC pulses, which do not yield a perfect rectangular function. However, the larger number of lobes, the more more accurate the slice

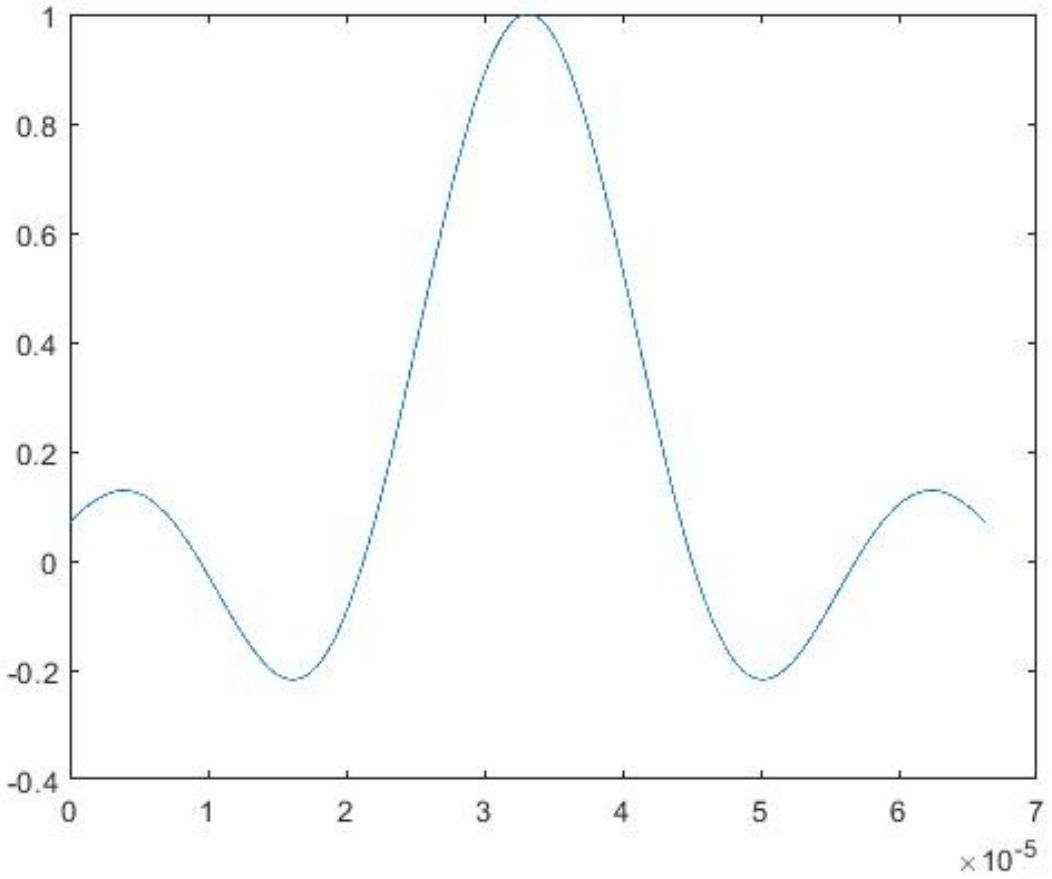

Figure 6: The shape of SINC function. The rectangular function fourier transforms into the SINC function.

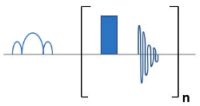

(a) A SINC pulse sequence. This pulse sequence is comprised of a SINC pulse with iterations of a 180° pulse and free induction decay

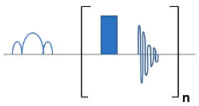

(b) A SINC pulse sequence. This pulse sequence is comprised of a SINC pulse and 90° pulse with iterations of a 180° pulse and free induction decay

Figure 7

profile.

A 200 µm slice has a pulse length of 100 µs, the shorter SINC pulse length used in these experiments. As shown in Figure 7a, the pulse sequence used is comprised of a SINC pulse, with repetitions of a 180° refocusing pulse FID. The SINC pulse only excites a specific region. The 180° is applied to the entire region, but only the initial slice profile is detected.

Alternatively, the SINC inversion pulse (I-SINC) sequence is also used for selective slice excitation. The entire range is detected, except the desired region, leaving a hole. This data is subtracted from the reference CPMG, resulting in cancellation of the undesired region. Figure 7b represents the pulse sequence for the I-SINC. It begins with a I-SINC pulse that excites only the desired region. The 90° pulse rotates the spins, such that the desired region is no longer detectable, and the rest of the sample is detectable. The pulse sequence ends with repetitions of a 180° pulse with FID.

2.5 Phase Shift

A SINC pulse has an underlying constant carrier frequency. The rectangular excitation pulse is centered at the carrier frequency. However, by altering the carrier frequency, the slice profile can be moved up or down. This is based on the Larmor frequency relationship, described as:

$$\omega = \gamma B_0 \tag{4}$$

Figure 8: Above the PM25 magnet, the magnetic field has a gradient. At positions further from the magnet, the magnetic field decreases.

γ is the gyromagnetic ratio, 42.577 MHz T^{-1}, for protons. The magnetic field has a gradient—the further from the magnet, the weaker the magnetic field, as shown in Figure 8. Because the gyromagnetic ratio is constant, as the frequency is decreased, the gradient also decreases. This relationship is what allows the correlation between position and frequency. As the carrier frequency of the SINC pulse is increased, the position of the slice profile moves down. Therefore identical SINC pulses with varying carrier frequencies will take identically shaped slice profiles at different positions in the sample. This allows for accurate characterization of multiple points within the 350 µm region. Multiple slice can be measured at a time by adding together each slices individual amplitudes and phases [14][15].

2.6 Hadamard Matrix

$$\begin{bmatrix} 1 & 1 & 1 & 1 \\ 1 & -1 & 1 & -1 \\ 1 & 1 & -1 & -1 \\ 1 & -1 & -1 & 1 \end{bmatrix}$$

A Hadamard matrix is a square matrix, comprised only of 1s and -1s as depicted above and can be $n \times n$ where n is a power of 2 [16]. In every Hadamard matrix, when placing two rows or columns side by side, half of the adjacent cells with have the same sign and

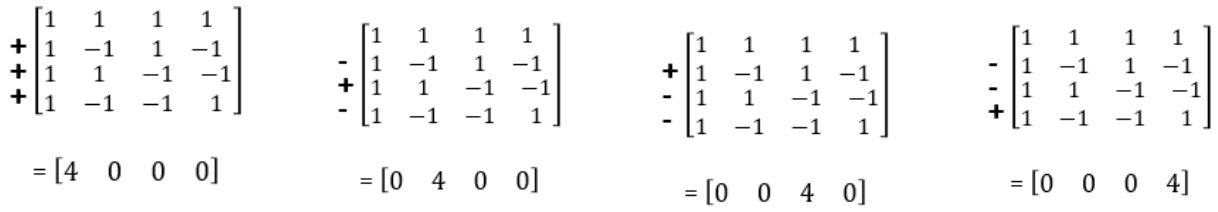

Figure 9: Hadamard Matrix Sequencing. By adding and subtracting different row, there is a maximum on one columns and 0s in the other three.

half of the adjacent cells will have a different sign. Rows within a Hadamard matrix can be added or subtracted together to maximize one position. With different combinations of addition and subtraction, each position can be maximized. When one position is maximized, the resultant row array is comprised of one 4 and three 0s, as shown in Figure 9[17]. The goal of using Hadamard matrix sequences is to limit the number of scans and still have a sufficient signal-to-noise ratio (SNR). As the number of scans increases the SNR decreases by the square root of the number of scans.

3 Methods

3.1 Experimentation

3.1.1 Methods with Hard Pulses

Six different methods were used to spatially encode the single-sided NMR, two of which use hard pulses and the remaining four use soft pulses. The first method is with a hard pulse, which is a short pulse that excites a large region. A CPMG pulse sequence was used to excite a region of 350 µm and the T_2 value of the entire region can be calculated from this data. The second method is profiling, which is a series of CPMGs at different depths. These experiments were done on the PM5, which has a lift that allows the magnet to move in a step-wise manner. As the lift moves up and down, the sensitive volume moves as well.

3.1.2 Methods with Soft Pulses

Another method of spatial encoding is with a soft pulse, which is a longer, shaped pulse that excites a smaller region. In this study, the SINC pulse is used to excite regions ranging from 50 µm to 200 µm. This SINC pulse can be offset in the positive or negative direction. When the SINC pulse is offset, the excitation frequency moves; however, the transmission frequency stays the same. The SINC pulse can be offset from 10 µm to 200 µm towards or away from the magnet. Closer to the magnet corresponds to the negative direction and farther away from the magnet corresponds to the positive direction. For both the SINC pulse and the offset SINC pulse, the T_2 values are measured for the specified excitation bandwidth. The fifth method of spatial encoding is via multiple slice excitation. Multiple SINC pulses can be layered on top of each other so individual offset SINC pulses do not need to be done. With the multiple slice excitation, one experiment can be run to measure up to 8 regions. The final method of spatial encoding is multiple slice excitation via Hadamard matrices. This is comprised of n number of experiments based on the $n \times n$ size of the matrix. All experiments were run on the PM25 except for the profiles because the PM25 does not have a lift associated with it. The T_2 value can be measured for each region within the Hadamard matrix. This study compares these six methods' ability to accurately measure T_2 as well as their respective efficiencies.

3.2 Samples

Within this study, experiments were run on four different materials. The first two materials, rubber and glycerol, were used because they give a large amount of signal, decreasing the experiment time and increasing efficiency. Acrylonitrile Butadiene Styrene (ABS) and Themoplastic Polyurethane (TPU) were used as well because both ABS and TPU can be 3D printed. Blocks of ABS and TPU were 3D printed at controlled lengths, widths, and heights. The measured T_2 values of these materials are outlined in Table 1. The T_2 values were measured via the CPMG pulse sequence on the PM25.

Material	T_2 value (ms)
Glycerol	12
Rubber	7
ABS	3.97
TPU	0.19

Table 1: This table represents important T_2 values of different materials in this study.

3.3 Generating Pulses

Pulse sequences are generated in the *TNMR* software. Figure 10 displays an example of the pulse sequence in the software. The pulse sequence begins with a phase reset of 5 µs and a start delay of 10 µs which are common to all pulse sequences in these experiments. Following this is the first pulse, which is either the 90° pulse or the SINC pulse, including both the amplitude and the phase. While the software already has hard pulses (90° and 180° pulses) programmed into it, soft pulses must be generated separately. The SINC pulses are generated via a Matlab script in Appendix B. The pulse generator creates SINC pulse amplitude and phase and account for offsets as well as phase flips for the Hadamard matrices. For a 90° pulse, the calibrated amplitude is 26 and for a 180° pulse, the calibrated amplitude is 52 for a pulse length of 6 µs. These values are calibrated specifically for the PM25 magnet and RF coil. After the first pulse is the first delay, which is calculated as follows:

$$\text{First Delay} = (\text{Echo Time}/2) - (90°\text{Pulse Width}/2) - (\text{SINC pulse length}/2) \tag{5}$$

The echo time corresponds to the amount of time in between each 180° iteration. The SINC pulse length is calculated via Eq. 2. The first delay time must be at least 40 µs so that the first and second pulses do not interfere with each other. The second pulse is a 180° pulse with an amplitude of 52 and a pulse width of 6 µs. The second delay is calculated as follows:

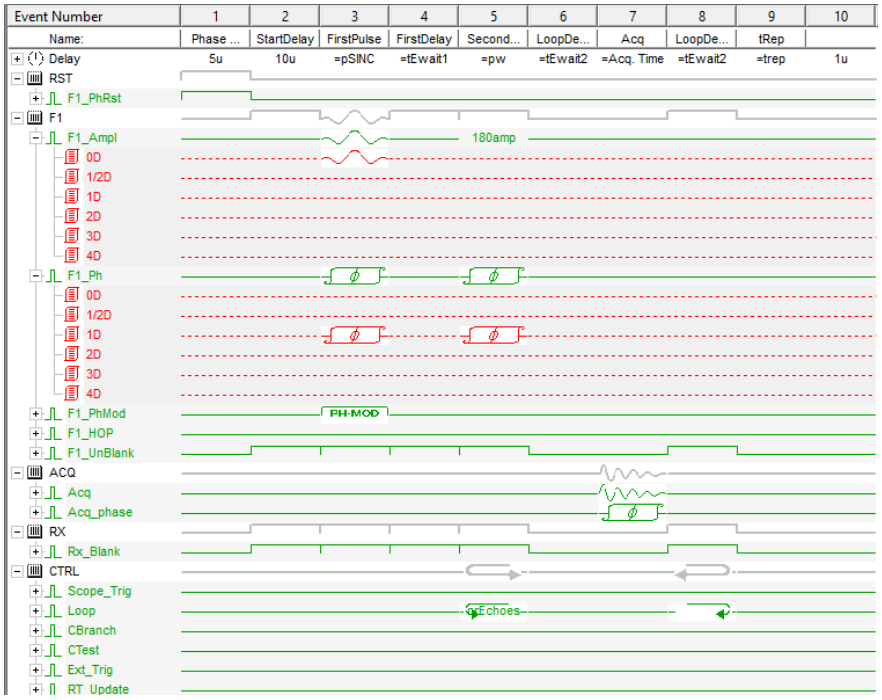

Figure 10: A screen-shot of designing a pulse sequence in TNMR. Pulse sequences are manually configured with specific pulse lengths and delays.

$$\text{Second Delay} = (\text{Echo Time}/2) - (90°\text{Pulse Width}/2) - (\text{Acquisition time}/2) \qquad (6)$$

After the second delay, the data is acquired and the second delay is repeated to allow for all the nuclei to relax in the transverse plan before the next 180° flip. The 180° pulse, second delay, acquisition, and repeated second delay are iterated n (number of echoes) times.

3.4 Data Processing

All data was processed in Matlab (Mathworks, Inc.; Natick, MA) scripts designed by Tyler Meldrum altered for these experiments. To visualize the excitation region, values were Fourier Transformed into the frequency domain, which can be converted into µm via Eq. 3. This gives signal amplitude as a function of position and regions excited will have some intensity as compared to regions not excited, which should have an intensity of zero. A

reference CPMG of glycerol was used to normalize the Fourier transforms. There is noise associated with the outer regions of the sensitive volume. The goal of normalization is to minimize subtract off the noise. This CPMG was fit to the function:

$$f(z) = e^{-\frac{(z-29.17)^2}{2*131.59^2}} \tag{7}$$

All normalization values less than 0.5 are set equal to 10^{10}. The data is divided by the normalization vector. This makes values on the edge of the region very close to zero and limits noise. Full width half max (FWHM) was used to to represent the width of data collected. This corresponds to the width of the peak at half of the maximum amplitude.

For T_2 processing, the data is fit via a T_2 mono-exponentially fitting script, included in Appendix B. For the Hadamard matrices, T_2 values are fit for each individual region.

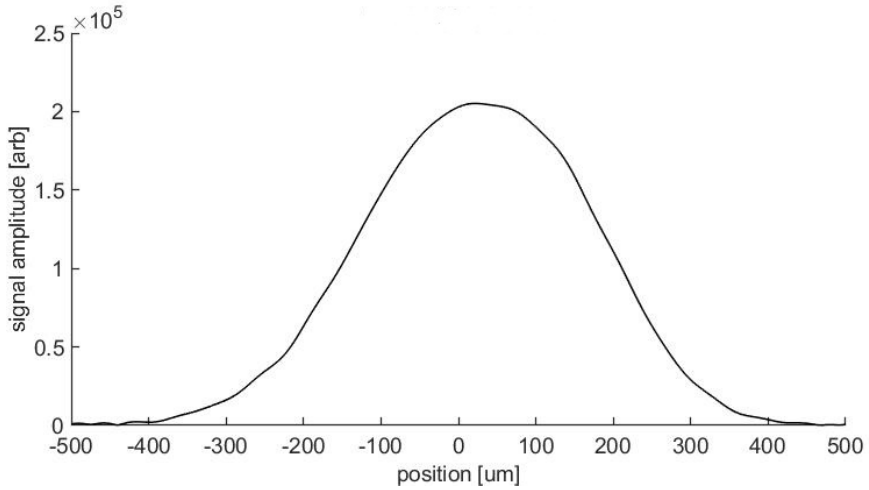

Figure 11: Fourier transform of a CPMG of glycerol on the PM25 with a FWHM of 358.85 µm.

4 Results and Discussion

4.1 Hard Pulse

As displayed in Figure 5, the short 6 µs pulse from the CPMG excited a wide, broad region. The rectangular function is Fourier Transformed into a SINC function. This CPMG has a FWHM of 358.85 µm. The excited region is centered approximately at 0 and encompasses the entire sensitivity region of the magnet. However, a 6 µs pulse excited a region of approximately 600 µm, but the RF coil is only able to transmit and receive a region of approximately 350 µm corresponding to a frequency of 100MHz, making the RF coil the limiting factor with hard pulses, as opposed to the hard pulses themselves.

As represented by Eq. 2, short pulses excite a large region and longer pulses excite a smaller region. In order to selectively excite a smaller region, a longer hard pulse can be used within the CPMG. When longer rectangular functions are Fourier Transformed into SINC functions, each lobe of the SINC function has a smaller width, but the same height. However, the lobes that neighbor the central lobe are larger and can cause less uniformity. Hard pulses can be used to excite larger regions, but are not preffered for exciting smaller regions.

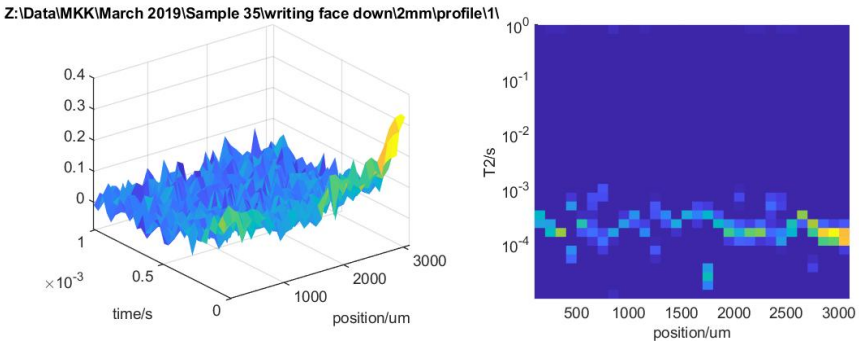

Figure 12: A profile on the PM5 of an epoxy and glass fiber. CPMGs were taken at 100 µm increments.

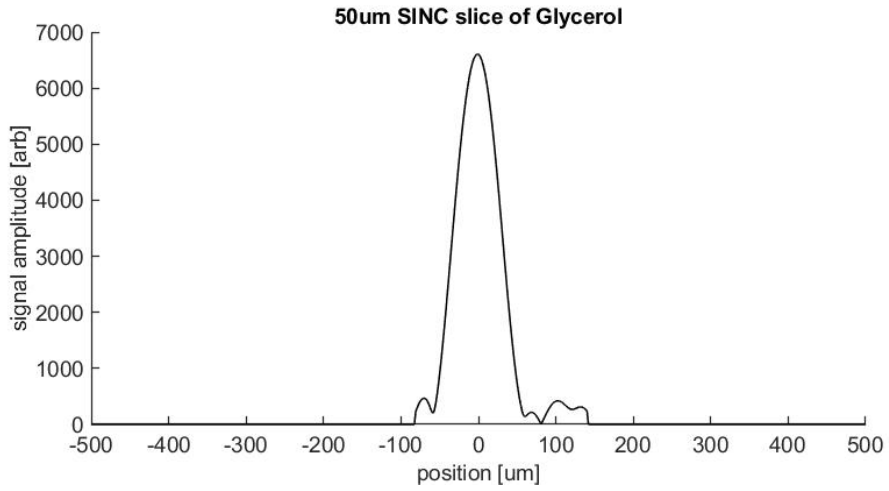

Figure 13: A 50 µm slice of glycerol centered at 0 µm. This data has a FWHM of 67.21 µm.

4.2 Profile

The profile in in Figure 12 was completed on epoxy and glass fibers on the PM5. This figure represents T_2 as a function of position in 100 µm increments. The interface between the epoxy and glass fiber is at 3000 µm and is characterized by a larger increase in intensity representing the aluminum. Profiles are beneficial because T_2 can be characterized in discrete increments relatively easily. However, it is a lengthy process and not ideal for efficiency. Profiles are also dependent on the precision of the lift, which can be unreliable.

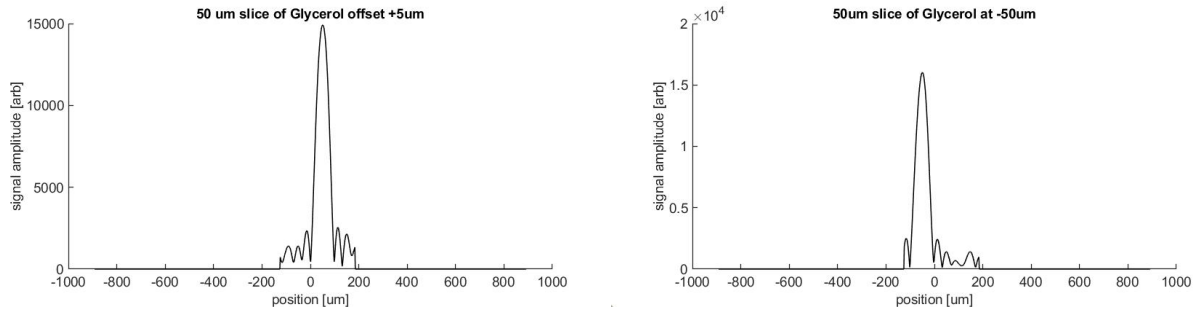

Figure 14: Two 50 µm SINC pulses offset at (a) 50 µm and (b) −50 µm. Both sets of data have a FWHM of 51.39 µm.

4.3 Soft Pulse

While hard pulses are dependent on the sensitivity of the RF coil, soft pulses are dependent solely on the sensitivity of the soft pulse as compared to hard pulses, which are dependent on the sensitivity of the coil. When a 50 µm region is expected to be excited by the pulse, the RF coil excites and receives that bandwidth. There are no limitations from the maximum bandwidth the RF coil can excite. Figure 13 displays the Fourier Transform of a 398 µs SINC pulse with normalization. The FWHM of this region is 67.21 µm. Figure 14 portrays two offset of positive 50 µm and negative 50 µm. These SINC pulses have the same amplitude as the SINC pulse in Figure 13, but a different phase. The FWHM for each of these is 51.39 µm. All of these SINC pulses were run on glycerol and normalized. Samples can be offset from −300 µm to 300 µm.

4.4 Multiple Slices

Figure 15 has eight different SINC slices from −275 µm to 250 µm in increments of 75 µm $(-275, -200, -125, -50, 25, 100, 175, 250)$. These SINC pulses were added together and run all at once. It is important to note that slices closer to the magnet tend to have higher signal, because they are closer to the RF coil. By exciting up to 8 regions at a time, the time it takes to measure samples discretely decreased by 8 times.

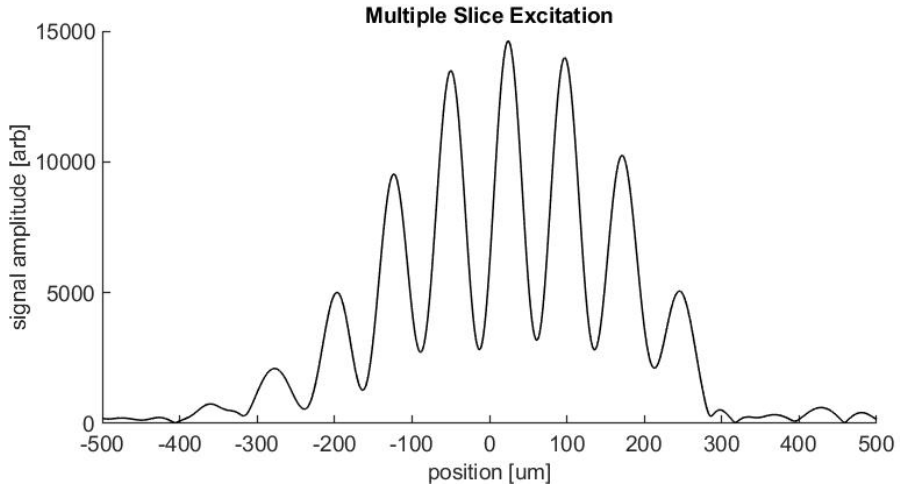

Figure 15: Eight different 50 µm SINC slices from −275 µm to 250 µm in increments of 75 µm (−275, −200, −125, −50, 25, 100, 175, 250).

4.5 4×4 Hadamard

A 4×4 Hadamard combination was run for 50 µm slices at −150 µm,−50 µm, 50 µm, 150 µm. This consisted of four different experiments with 180° flips in each phase corresponding to the Hadamard Matrix. These results are represented by the black line in 16. Each Hadamard pulse was run with 1024 scans for a total of 8196 scans. The red lines in Figure 16 represent individual SINC pulse experiments at their respective centers, each completed with 1024 scans for a total of 8196 scans. The ratio of the integration of the Hadamard to the individual slice was calculated for each slice respectively. The expected ratio for each slice is 2, because the Hadamard matrix experiments have four times the number of scans and SNR decreases as the square root of the number of scans.

4.6 8×8 Hadamard

Figure 17 displays an 8×8 Hadamard sequencing on rubber for 50 µm slices centered at −275 µm, −200 µm, −125 µm, −50 µm, 25 µm, 100 µm, 175 µm, and 250 µm. The slices closer to the center have more signal, whereas the slices farther away from the center have less signal because there is less sensitivity of the RF coil father away from the magnet.

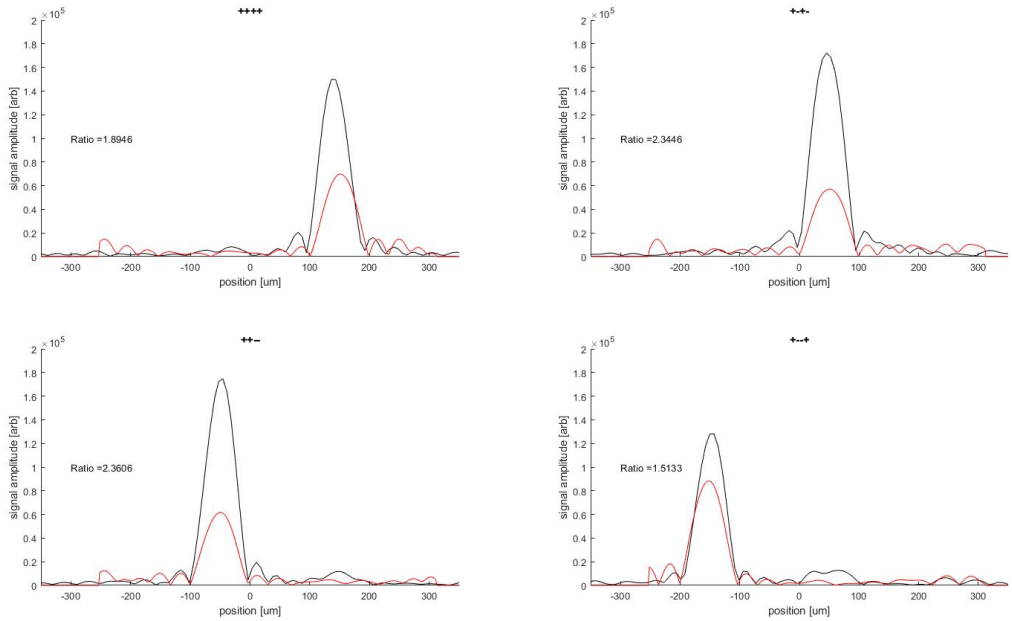

Figure 16: This figure represents a comparison between the Hadamard pulse sequence (black line) and individual SINC pulses (red line).

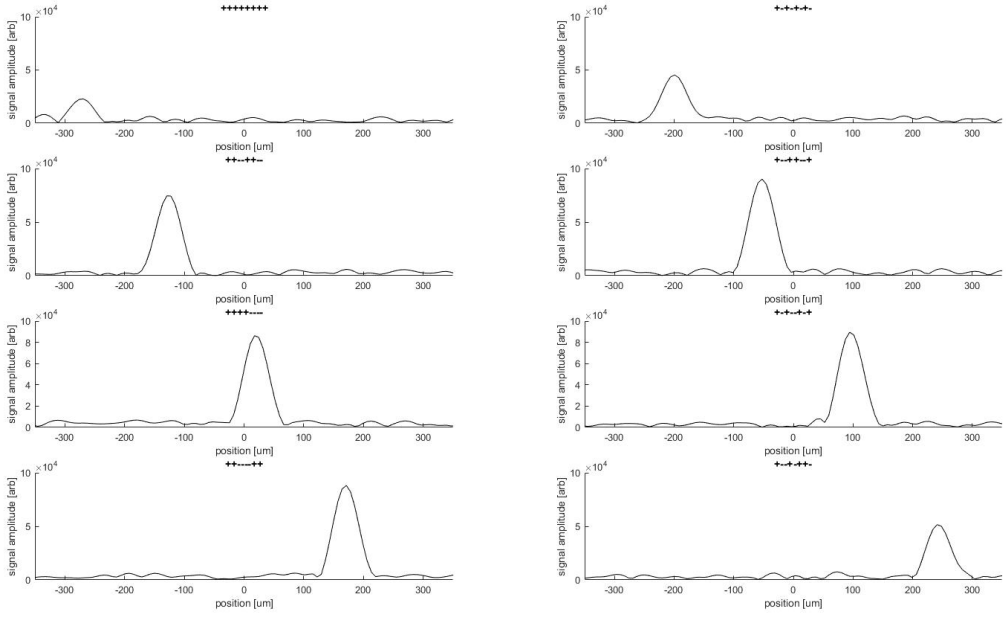

Figure 17: This is an 8×8 Hadmard series on rubber with 50 µm slices at −275 µm, −200 µm, −125 µm, −50 µm, 25 µm, 100 µm, 175 µm, and 250 µm.

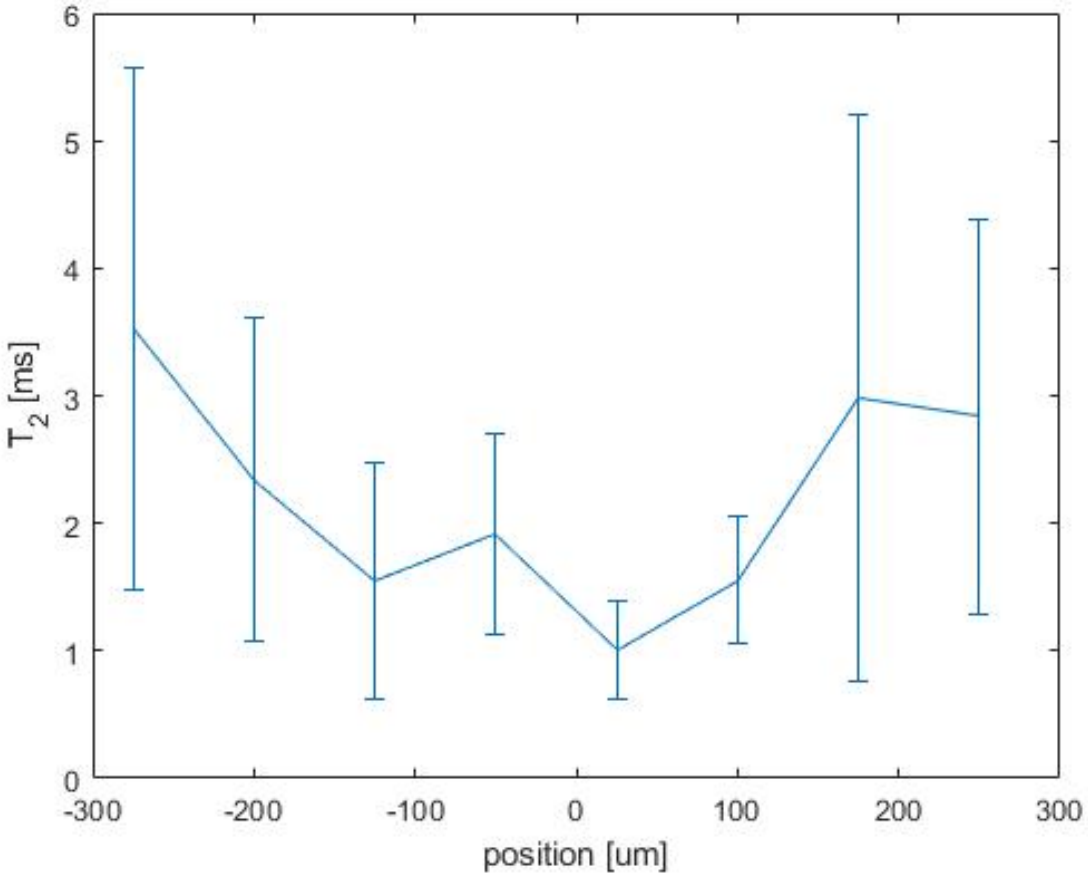

Figure 18: This figure represents the T_2 values of rubber at positions $-275\,\mu m$, $-200\,\mu m$, $-125\,\mu m$, $-50\,\mu m$, $25\,\mu m$, $100\,\mu m$, $175\,\mu m$, and $250\,\mu m$ for an 8×8 Hadamard sequence.

The T_2 values of each slice are represented in Figure 18. These T_2 are constant and range from 2.0 ms to 5.2 ms. These values compare to the expected value of 3.43 ms, which was measured from a single T_2 fitting of a $50\,\mu m$ SINC pulse on rubber centered at $0\,\mu m$. Figure 19 represents the same 8×8 Hadamard matrix addition and subtractions on glycerol. These T_2 values compare to an expected values of 19.1 ms. The T_2 values for rubber and glycerol are different from each other, but consistent within each material. Glycerol has a longer T_2 because glycerol has less rigid molecules than rubber. Therefore, the molecules are more rapidly moving.

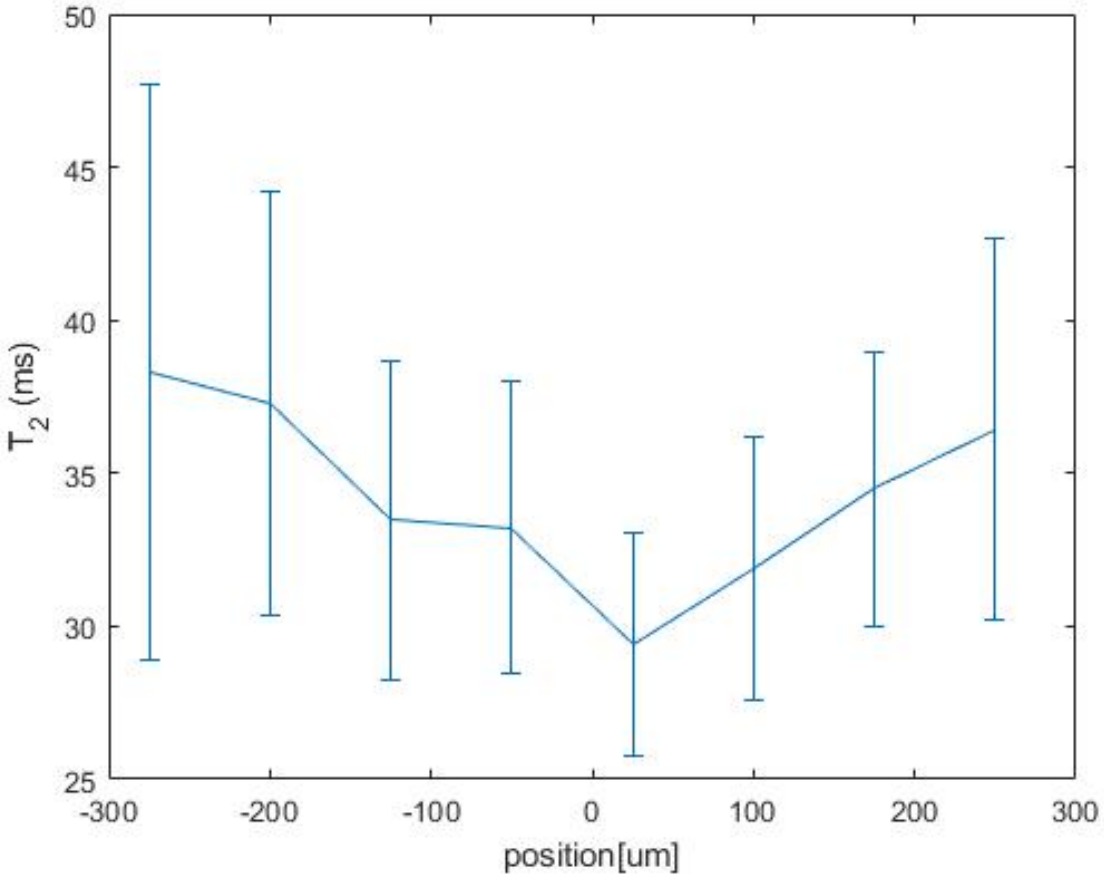

Figure 19: This figure represents the T_2 values of glycerol at positions $-275\,\mu m$, $-200\,\mu m$, $-125\,\mu m$, $-50\,\mu m$, $25\,\mu m$, $100\,\mu m$, $175\,\mu m$, and $250\,\mu m$ for an 8×8 Hadamard sequence.

5 Conclusion

Six different methods for spatial encoding were successfully implemented and analyzed for accuracy and efficiency. The hard pulse (CPMG) is sufficient for measuring larger regions. A 6 µs pulse yields a FWHM of 358 µm. The profile allows for spatial resolution with a hard pulse, but is extensive and inefficient. The soft pulse is better suited for smaller slices and can be be offset in the positive and negative directions. The FWHM of the offset slices was 31.5 µm. By adding the SINC pulses together, multiple slices are excited at once. Up to eight slices can be excited at once with adequate peak resolution.

Up to an 8×8 Hadamard Matrix sequence can be implemented on the PM25 magnet within the 350 μm regions. The ratio of the integration of these peaks to the integration of individual SINC slices is above 4 (expected value) for each slice −150 µm,−50 µm, 50 µm, 150 µm. The T_2 values for each slice in a 8×8 Hadamard matrix sequence remains constant for both glycerol and rubber.

6 References

References

[1] R. Haken, B. Bluemich, Anisotropy in tendon investigated in vivo by a portable nmr scanner, the nmr-mouse, Journal of magnetic resonance (San Diego, Calif. : 1997) 144 (2000) 195–9. doi:10.1006/jmre.2000.2040.

[2] D. Gerlach, M. Trammer, J. Zange, Evaluation of a mobile nmr sensor for determining skin layers and locally estimating the t2eff relaxation time in the lower arm, Magma (New York, N.Y.) 25. doi:10.1007/s10334-012-0317-8.

[3] N. Halmen, C. Kugler, E. Kraus, B. Baudrit, T. Hochrein, M. Bastian, Single-sided nmr for the measurement of the degree of cross-linking and curing, Journal of Sensors and Sensor Systems 7 (2018) 21–30. doi:10.5194/jsss-7-21-2018.

[4] B. Bluemich, F. Casanova, J. Perlo, F. Presciutti, C. Anselmi, B. Doherty, Noninvasive testing of art and cultural heritage by mobile nmr, Accounts of chemical research 43 (2010) 761–70. doi:10.1021/ar900277h.

[5] M. Baias, Mobile nmr: An essential tool for protecting our cultural heritage, Magnetic Resonance in Chemistry 55 (1) (2017) 33–37.

[6] J. Keeler, Understanding NMR spectroscopy / James Keeler., 2nd Edition, John Wiley and Sons, Chichester, U.K., 2010.

[7] A. ur Rahman, M. I. Choudhary, A. tul Wahab, Chapter 4 - spin-echo and polarization transfer, in: A. ur Rahman, M. I. Choudhary, A. tul Wahab (Eds.), Solving Problems with NMR Spectroscopy (Second Edition), second edition Edition, Academic Press, Boston, 2016, pp. 133 – 190. doi:https://doi.org/10.1016/B978-0-12-411589-7.00004-8.
URL http://www.sciencedirect.com/science/article/pii/B9780124115897000048

[8] C. Laule, A. MacKay, Chapter 3.5 - t2 relaxation, in: J. Cohen-Adad, C. A. Wheeler-Kingshott (Eds.), Quantitative MRI of the Spinal Cord, Academic Press, San Diego, 2014, pp. 181 – 206. doi:https://doi.org/10.1016/B978-0-12-396973-6.00013-7.
URL http://www.sciencedirect.com/science/article/pii/B9780123969736000137

[9] S. B. Damelin, W. Miller, The fourier transform, in: The Mathematics of Signal Processing, Cambridge University Press, Cambridge, 2011, pp. 127–163.

[10] A. G. Marshall, Fourier transforms in NMR, optical, and mass spectrometry : a user's handbook / Alan G. Marshall and Francis R. Verdun., Elsevier, Amsterdam ; New York, 1990.

[11] B. B. F. Casanova, J. Perlo, Single-Sided NMR, Springer, 2011.

[12] S. A. Hertel, D. W. de Kort, I. Bush, A. J. Sederman, L. F. Gladden, B. Anger, H. de Jong, M. Appel, Fast spatially-resolved t2 measurements with constant-gradient cpmg, Magnetic Resonance Imaging 56 (2019) 70 – 76, porous Media. doi:https://doi.org/10.1016/j.mri.2018.09.003.
URL http://www.sciencedirect.com/science/article/pii/S0730725X18304387

[13] H. Taga, A modulation scheme with rectangular frequency spectrum based on truncated sinc pulse, in: 2013 6th IEEE/International Conference on Advanced Infocomm Technology (ICAIT), 2013, pp. 61–62.

[14] S. Müller, Multifrequency selective rf pulses for multislice mr imaging, Magnetic Resonance in Medicine 6 (3) (1988) 364–371. arXiv:https://onlinelibrary.wiley.com/doi/pdf/10.1002/mrm.1910060315, doi:10.1002/mrm.1910060315.
URL https://onlinelibrary.wiley.com/doi/abs/10.1002/mrm.1910060315

[15] S. Abo Seada, A. N. Price, J. V. Hajnal, S. J. Malik, Optimized amplitude modulated multiband rf pulse design, Magnetic Resonance in Medicine 78 (6)

(2017) 2185–2193. arXiv:https://onlinelibrary.wiley.com/doi/pdf/10.1002/mrm.26610, doi:10.1002/mrm.26610.

URL https://onlinelibrary.wiley.com/doi/abs/10.1002/mrm.26610

[16] A. T. Butson, Generalized hadamard matrices, Proceedings of the American Mathematical Society 13 (6) (1962) 894–898.

URL http://www.jstor.org/stable/2034082

[17] A. Tal, B. Shapira, L. Frydman, Single-scan 2d hadamard nmr spectroscopy, Angewandte Chemie International Edition 48 (15) (2009) 2732–2736. arXiv:https://onlinelibrary.wiley.com/doi/pdf/10.1002/anie.200805612, doi:10.1002/anie.200805612.

URL https://onlinelibrary.wiley.com/doi/abs/10.1002/anie.200805612

A Data Tables

Glycerol T_2 Relaxation Data		
Position(µm)	T_2 (ms)	T_2 Error (ms)
-275	38.3079	9.422
-200	37.2506	6.9274
-125	33.4613	5.2208
-50	33.2233	4.7931
25	29.4147	3.6648
100	31.8811	4.3192
175	34.4771	4.5073
250	36.4327	6.2341

Rubber T_2 Relaxation Data		
Position(µm)	T_2 (ms)	T_2 Error (ms)
-275	5.2184	1.3626
-200	4.0445	1.0354
-125	2.4039	0.9459
-50	2.5881	1.1271
25	2.0052	0.824
100	2.3452	0.8963
175	3.0811	1.2044
250	3.4522	0.7931

B MATLAB Scripts

Script 1: Pulse Generation

SINC pulse Generator (can be used with or without Hadamard Sequencing)—created by Tyler Meldrum, edited by Madeline Brass.

`Had_generator.m`

```
% SINC amplitude table generator for Tecmag
clear
clc
close all

%%%%%%% User-defined parameters %%%%%%%
slice = 0.05; %mm, slice thickness
G = 6.59; %T m-1, B0 field gradient
bandwidth_factor = 5.58;
integral_factor = 0.18;
dt = 1e-8; %s, time per pulse point
offset = -[-0.05 0.05]; %mm positive indicates down, negative indicates up
phase = [0 0];
hard90time = 6E-6; %s
hard90power = 26;
apo = 1; %apodization on or off
%%%%%%% END User-defined parameters %%%%%%%

gamma = 42.576; %MHz T-1
SW = slice*G*gamma*1000; %Hz
offset_Hz = offset*G*gamma*1000; %Hz
offset_rad = offset_Hz*2*pi;
phase_rad = mod(phase*(pi/2),2*pi);
tau = bandwidth_factor/SW; %pw in s
```

```
25
26 fprintf('%.0f um slice\nSINC pulse length = %.2f us\n',1e3*slice,tau*1e6);
27
28 N = round(tau/dt); %number of points per pulse waveform
29
30 if apo == 1
31     apo_fac = hamming(N)';
32 else
33     apo_fac = 1;
34 end
35
36 amp = hard90power*hard90time/tau/integral_factor;
37
38 pulse_time = -N*dt/2+dt/2:dt:N*dt/2-dt/2;
39 B1 = apo_fac.*amp.*sinc(SW*pulse_time);
40
41 for ii = 1:numel(offset)
42     B1_mod(:,ii) = B1'.*exp(1j*(offset_rad(ii))*pulse_time').*exp(1j*-
          phase_rad(ii));
43 end
44
45 pulse = sum(B1_mod,2);
46
47 pulse_rf = abs(pulse);
48 pulse_ph = angle(pulse);
49 pulse_ph_wrap = pulse_ph<0;
50 pulse_ph_deg = (360/(2*pi))*(pulse_ph + 2*pi*pulse_ph_wrap);
51
52 figure(1); hold on; plot(real(pulse)); plot(imag(pulse))
53
54 hh = figure(2);
55 subplot(2,1,1)
56 plot(pulse_time,pulse_rf);
```

```
57 ylabel('rf amp [arb]')
58 subplot(2,1,2)
59 plot(pulse_time,pulse_ph_deg);
60 xlabel('time [s]')
61 ylabel('rf phase [deg]')
62 pubgraph(hh,14,1,'w','Arial');
63
64 dlmwrite('SINC_Amp_new.dat',pulse_rf);
65 dlmwrite('SINC_Phase_new.dat',pulse_ph_deg);
```

Script 2: Data Processing

T_2 processing and Fourier transform script - created by Tyler Meldrum, edited by Madeline Brass

`HadamardT2_FT.m`

```
% clear
% clc
close all

%%
filenameA = 'SINC50_4_4Feb2018'; %0000
filenameB = 'SINC50_5_4Feb2018'; %0202
filenameC = 'SINC50_6_4Feb2018'; %0022
filenameD = 'SINC50_7_4Feb2018'; %0220

filedir = 'C:\CommonData\MRB\SINC_pulse\Glycerol\';
filelocA = strcat(filedir,filenameA);
filelocB = strcat(filedir,filenameB);
filelocC = strcat(filedir,filenameC);
filelocD = strcat(filedir,filenameD);

[apA,specA,spec2A,spec3A,spec4A] = readTecmag4d(strcat(filelocA,'.tnt'));
[apB,specB,spec2B,spec3B,spec4B] = readTecmag4d(strcat(filelocB,'.tnt'));
[apC,specC,spec2C,spec3C,spec4C] = readTecmag4d(strcat(filelocC,'.tnt'));
[apD,specD,spec2D,spec3D,spec4D] = readTecmag4d(strcat(filelocD,'.tnt'));

tEcho = 500; %Echotime (us)
nEchoes = 128; %Number of echoes
nPts = apA.ctd;
tD = apA.dw(1);
nPtsBlank = 0; %Don't touch
```

```
27
28 zf = 2; %zero filling... Don't touch
29 G = 6.59;                              % Gradient (T m-1)
30 gamma = 42.576;                        % MHz T-1
31 gammaRad = gamma*2*pi*1e6;             % rad s-1 T-1
32
33 %%
34 echoVector = (tEcho:tEcho:nEchoes*tEcho)*1e-6;
35
36 dataA = reshape(specA,nPts,nEchoes);
37 dataA = dataA((nPtsBlank+1):(nPts-nPtsBlank),:);
38 dataIntA = sum(dataA,1);
39 dataIntReA = real(dataIntA)./max(real(dataIntA));
40 dataIntImA = imag(dataIntA)./max(real(dataIntA));
41
42 dataB = reshape(specB,nPts,nEchoes);
43 dataB = dataB((nPtsBlank+1):(nPts-nPtsBlank),:);
44 dataIntB = sum(dataB,1);
45 dataIntReB = real(dataIntB)./max(real(dataIntB));
46 dataIntImB = imag(dataIntB)./max(real(dataIntB));
47
48 dataC = reshape(specC,nPts,nEchoes);
49 dataC = dataC((nPtsBlank+1):(nPts-nPtsBlank),:);
50 dataIntC = sum(dataC,1);
51 dataIntReC = real(dataIntC)./max(real(dataIntC));
52 dataIntImC = imag(dataIntC)./max(real(dataIntC));
53
54 dataD = reshape(specD,nPts,nEchoes);
55 dataD = dataD((nPtsBlank+1):(nPts-nPtsBlank),:);
56 dataIntD = sum(dataD,1);
57 dataIntReD = real(dataIntD)./max(real(dataIntD));
58 dataIntImD = imag(dataIntD)./max(real(dataIntD));
59 %%
```

```
60
61 Fs = 1/tD;                              % Sampling frequency
62 L = (nPts)*(2^zf);           % Length of signal
63 NFFT = 2^nextpow2(L);                % Next power of 2 from length of y
64
65 t = (-(L-1)/2:L/2)*tD;                % Time vector
66 f = linspace(-Fs/2,Fs/2,NFFT);       % Hz
67 z = f/(gamma*G);                      % um, 280.47 Hz/um (for PM25)
68
69 %normalize
70 z_norm = exp(-(z-29.17).^2./(2*131.59^2));
71 z_norm(z_norm<0.05) = 1e10;
72
73 datA = padarray(dataA, size(dataA(:,1),1)/2*((2^zf)-1),0); % Pad with 0's
74 datB = padarray(dataB, size(dataB(:,1),1)/2*((2^zf)-1),0); % Pad with 0's
75 datC = padarray(dataC, size(dataC(:,1),1)/2*((2^zf)-1),0); % Pad with 0's
76 datD = padarray(dataD, size(dataD(:,1),1)/2*((2^zf)-1),0); % Pad with 0's
77
78 profilesA = flipud(fftshift(fft(datA,NFFT)/L, 1)); % Performs FFT algorithm
79 profilesB = flipud(fftshift(fft(datB,NFFT)/L, 1)); % Performs FFT algorithm
80 profilesC = flipud(fftshift(fft(datC,NFFT)/L, 1)); % Performs FFT algorithm
81 profilesD = flipud(fftshift(fft(datD,NFFT)/L, 1)); % Performs FFT algorithm
82
83 profilesAA = abs(profilesA+profilesB+profilesC+profilesD);
84 profilesBB = abs(profilesA-profilesB+profilesC-profilesD);
85 profilesCC = abs(profilesA+profilesB-profilesC-profilesD);
86 profilesDD = abs(profilesA-profilesB-profilesC+profilesD);
87 %%
88
89 dataIntA = sum(abs(profilesAA),1);
90 dataIntB = sum(abs(profilesBB),1);
91 dataIntC = sum(abs(profilesCC),1);
92 dataIntD = sum(abs(profilesDD),1);
```

```
93  %
94  dataIntAll = [dataIntA; dataIntB; dataIntC; dataIntD;];
95  dataIntAllAbs = abs(dataIntAll./max(dataIntAll,[],2));
96
97  guess = [1 12e-3 0.02];% 0.6 6e-03];
98  for ll = 1:4
99      [beta(:,ll),R,J,CovB(:,:,ll)] = nlinfit(echoVector,dataIntAllAbs(ll,:),
            @t2monofit, guess);
100     ypred(ll,:) = t2monofit(beta(:,ll),echoVector);
101     ci(:,:,ll) = nlparci(beta(:,ll),R,'jacobian',J);
102 end
103
104 T2 = beta(2,:)*1e3; %ms
105 T2_err = (beta(2,:)-squeeze(ci(2,1,:))')*1e3;
106 z_hadamard = [-150 -50 50 150];
107
108 gg = figure(2);
109 errorbar(z_hadamard,T2,T2_err);
110 xlim([-300 300])
111 %
112 close all
113
114 xlims = [-350 350];
115 ylims = [0 2e5];
116
117 % for a 4x4 matrix
118 hh = figure(2);
119 subplot(2,2,1);
120 set(gcf,'Position',[560   530   860   420])
121 hold on
122 plot(z,abs(profilesAA(:,2)),'-k');
123 plot(z2,abs(had150),'-r');
124 xlim(xlims);
```

```
ylim(ylims);
xlabel('position [um]')
ylabel('signal amplitude [arb]')
title('++++','Interpreter','None')
A = trapz(z,abs(profilesAA(:,2)));
B = trapz(z2,abs(had150));
ratio = A./B
ratiostr = ['Ratio =',num2str(ratio)];
text(-300,1e5,ratiostr)
print(strcat(filedir,filenameA,'_FTprofileAA.jpg'),'-djpeg')

hh = subplot(2,2,2);
set(gcf,'Position',[560   530   860   420])
hold on
plot(z,abs(profilesBB(:,2)),'-k');
plot(z2,abs(had50),'-r');
xlim(xlims);
ylim(ylims);
xlabel('position [um]')
ylabel('signal amplitude [arb]')
title('+-+-','Interpreter','None')
C = trapz(z,abs(profilesBB(:,2)));
D = trapz(z2,abs(had150));
ratio1 = C./D
ratiostr = ['Ratio =',num2str(ratio1)];
text(-300,1e5,ratiostr)
print(strcat(filedir,filenameB,'_FTprofileBB.jpg'),'-djpeg')

hh = subplot(2,2,3);
set(gcf,'Position',[560   530   860   420])
hold on
plot(z,abs(profilesCC(:,2)),'-k');
plot(z2,abs(hadn50),'-r');
```

```
158 xlim(xlims);
159 ylim(ylims);
160 xlabel('position [um]')
161 ylabel('signal amplitude [arb]')
162 title('++--','Interpreter','None');
163 E = trapz(z,abs(profilesCC(:,2)));
164 F = trapz(z2,abs(hadn50));
165 ratio2 = E./F
166 ratiostr = ['Ratio =',num2str(ratio2)];
167 text(-300,1e5,ratiostr)
168 print(strcat(filedir,filenameC,'_FTprofileCC.jpg'),'-djpeg')
169
170 hh = subplot(2,2,4);
171 set(gcf,'Position',[560   530   860   420])
172 hold on
173 plot(z,abs(profilesDD(:,2)),'-k');
174 plot(z2,abs(hadn150),'-r');
175 xlim(xlims);
176 ylim(ylims);
177 xlabel('position [um]')
178 ylabel('signal amplitude [arb]')
179 title('+--+','Interpreter','None')
180 G= trapz(z,abs(profilesDD(:,2)));
181 H = trapz(z2,abs(hadn150));
182 ratio3 = G./H
183 ratiostr = ['Ratio =',num2str(ratio3)];
184 text(-300,1e5,ratiostr)
185 print(strcat(filedir,filenameD,'_FTprofileDD.jpg'),'-djpeg')
186 %%
```